Time-correlated Geometrical Radio Propagation Model for LEO-to-Ground Satellite Systems

Martinez, Enric Juan; Rodriguez, Ignacio; Lauridsen, Mads; Wigard, Jeroen; E. Mogensen, Preben

Published in:
2021 IEEE 94th Vehicular Technology Conference, VTC 2021-Fall - Proceedings

DOI (link to publication from Publisher):
10.1109/VTC2021-Fall52928.2021.9625273

Publication date:
2021

Document Version
Accepted author manuscript, peer reviewed version

Time-correlated Geometrical Radio Propagation Model for LEO-to-Ground Satellite Systems

Enric Juan*, Ignacio Rodriguez*, Mads Lauridsen†, Jeroen Wigard † and Preben Mogensen*†
*Wireless Communication Networks Section, Department of Electronic Systems, Aalborg University, Denmark
†Nokia, Aalborg, Denmark
‡ejm@es.aau.dk

***Abstract*—Low-Earth orbit (LEO)-based satellite communication systems are envisioned to be a next-generation key asset for telecom industry due to their potential to deliver global and seamless mobile broadband services. The high-speed mobility relative to Earth, that characterizes LEO orbits, will pose time-varying propagation conditions impacting the system performance in terms of mobility, availability and user throughput. Therefore, in LEO satellite systems, it is fundamental to understand accurately the signal variations between mobile satellites and users on the ground. This paper presents a radio propagation model able to describe realistically the time variations of the LEO-to-Ground path loss, including the line-of-sight changes and the impact of the surrounding built-up structures. We propose a low-complexity geometrical approach based on intelligent ray-tracing that considers the general dependencies on the elevation angle. The resulting model has been validated for a suburban scenario, exhibiting an overall root mean square error of 1.1 dB. Furthermore, the time-correlated geometry-based model is suitable for system-level radio mobility simulations with LEO-to-Ground satellite systems.**

I. Introduction

Low Earth orbit (LEO) satellite networks have become a reality with the initial deployments of constellations by SpaceX and OneWeb. Driven by the development of new low-cost space technologies and the reduction of launching costs, space is a rising market with many new players convinced of its potential [1]. Organizations and companies in the 3rd Generation Partnership Project (3GPP) continue working towards the integration of satellites into 5G networks, which aim at meeting the high-demand for internet services by providing global and seamless broadband access. Proof of this is the completion of two study items [2] [3] for Rel-15 and Rel-16 and the ongoing work item [4] for Rel-17.

The deployment of satellite constellations at relatively low altitude, between $600\,\mathrm{km}$ and $1200\,\mathrm{km}$, has unique capabilities such as a reduced latency and a more favourable link budget compared to higher orbits like the geostationary orbit (i.e. $35.786\,\mathrm{km}$ height). A key challenge for LEO-based systems is the rapid movement of the satellites with respect to the Earth's surface, i.e. approximately $7.5\,\mathrm{km/s}$. Even for ground stationary user equipments (UEs), this translates into fast and continuous changes of the propagation conditions which have a clear impact on the system performance.

To enable LEO-based 5G access, it is paramount to understand and address the time-varying dynamics of the radio propagation links between LEO systems and the UEs on the ground. Many research efforts have acknowledged the importance of the channel modelling, however, satellite-to-ground channels, considering time-varying satellite mobility, have not received as much attention as in terrestrial deployments. The most relevant and up-to-date studies are the works done by the International Telecommunications Union (ITU) and the 3GPP. In the report P.681 [5], the ITU defines its recommendations to predict the propagation impairments in the land mobile-satellite links. Even though the model includes some considerations regarding LEO satellites, only UE mobility is considered. On the other hand, 3GPP addressed the channel modelling for non-terrestrial network (NTN) in [2]. Despite the technical report considers model parameters for LEO satellites such as the probability of line-of-sight (LOS), clutter loss and shadow fading, movement of the satellites is not supported. Hence, the model does not define the correlations over time of the channel parameters.

Modelling the time correlations is fundamental to facilitate the design, development and planning of LEO-based NTN, as the mobility performance of the system needs to be carefully evaluated to ensure satisfactory end user experience. In [6] we conducted system-level simulations to evaluate the 5G New Radio mobility performance in LEO-based NTN, where we had to assume a constant LOS for the satellite-to-UE links due to the lack of a suitable channel model in terms of mobility. Later on, initial steps were done towards a model able to capture the time correlations in [7], where we proposed a Markov-based model to realistically determine the LOS state transitions. In this paper, we complete our previous work by proposing a model that predicts the signal strength variations caused by effect of LOS obstructions considering stationary users on the ground and mobile satellites. The model describes the path loss and the shadow fading as a function of a given channel state transition point. The model is built on the basis of models for terrestrial radio deployments to define how the diffraction and reflection physical phenomena changes over elevation angle. Furthermore, the developed large-scale propagation model is able to achieve a compromise between accuracy and simplicity resulting in a useful extension to the channel model for NTN reported by the 3GPP.

The remainder of the paper is structured as follows: Section II introduces the terrestrial models used as a baseline for our model. Section III describes our proposed geometrical model and illustrates its dynamics. The ray-tracing simulations used

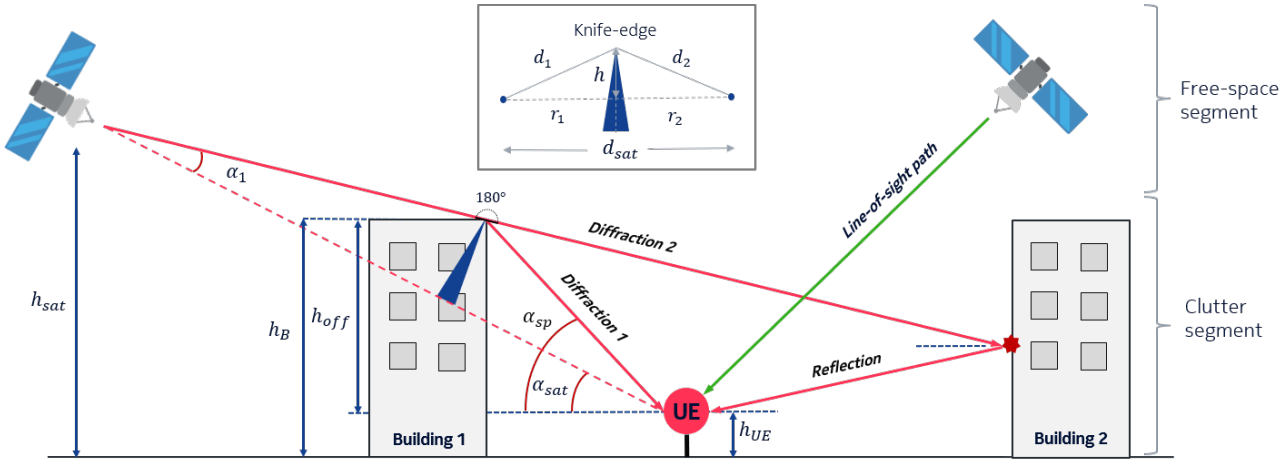

Fig. 1: Geometric concept to illustrate the radio wave interactions of LEO-to-ground links.

for validation of the model are presented in Section IV, while in Section V we discuss the overall accuracy of the model. Section VI elaborates on the extraction of applicable shadow fading parameters and, finally, VII concludes the paper.

II. Baseline Radio Propagation Models

Several terrestrial radio propagation models have described radio link situations in built-up areas that are close to the one experienced in the LEO-to-Ground scenario. Hereafter, we provide a brief description of the models used as baseline for developing our model.

A. Knife-edge diffraction model

The ITU collected in its recommendation P.526 [8] several models to study the effect of diffraction on the received field strength, including the widely used model known as knife-edge diffraction. This model ignores the roughness of the material by considering an ideal and infinite edge and adjusts the loss based on the dimensionless parameter v (see [8, Eq. (26-29)]). Further details of this parameter are discussed in Section III.

B. Ikegami and Walfisch models

Ikegami *et al.* published in [9] a model based on geometrical optics assuming a simple two-ray approach; a direct rooftop-to-street diffracted ray and a ray reflected by a building across the street. Later on, Walfisch and Bertoni proposed in [10] a model addressing the impact of buildings in the propagation between base stations and UEs. Both models were later combined in [11] to address the limitations of each individual model. Nonetheless, the accuracy of the resulting model is limited to an environment where the range of parameters such as the slant range and the transmitter antenna height are up to $5\,\mathrm{km}$ and $50\,\mathrm{m}$, respectively.

III. Proposed Geometrical Model

A. Geometry description

Radio signals from LEO satellites can be attenuated by buildings located near the UE. These signals propagate blockage-free over long distances and interact with the built-up area prior to reaching the UE. We denote the free-space segment as the path that the radio signal covers under free-space conditions, while we refer to the clutter segment as the portion of the path where the signal propagates in built-up areas. This scenario is depicted in Fig. 1, where the LEO satellite is at an altitude of h_{sat}, at a distance d_{sat} and with an elevation angle of α_{sat} with regards to the UE, located at a height of h_{UE} surrounded by buildings. The LOS path is obstructed by *Building 1* with a height of h_B. The signal reaches the rooftop of *Building 1* with angle α_1, measured from the satellite-UE plane, and grazes towards the UE with angle α_{sp}. We term α_{sp} as the *switching point* because the angle denotes the line between NLOS and LOS conditions.

The model assumes a geometrical approach based on two-rays: a ray diffracted at the rooftop of *Building 1* and a ray reflected by *Building 2* after grazing over *Building 1*. For further clarification, both rays are illustrated in Fig. 1. We assume *Diffraction 1* varies depending on angles α_1, α_{sat} and α_{sp}, while *Diffraction 2* remains constant with the edge of *Building 1* just in line between the satellite and the reflection spot on *Building 2*.

B. Formulation

Following the scenario just described, the overall path loss (PL) is estimated in Eq. 1 according to the channel conditions. We use the model in [7] to generate time-correlated LOS and NLOS states as a function of α_{sat} and define the values of α_{sp}. Once the LOS/NLOS states are computed, the geometrical-based radio propagation loss is calculated for the different states by splitting PL in three components: free-space L_{FS}, clutter L_C and shadow fading χ, where L_C is negligible when the UE is in LOS conditions.

$$PL = \begin{cases} L_{FS} + \chi, & \text{if LOS} \\ L_{FS} + L_C + \chi, & \text{if NLOS} \end{cases} \quad [\mathrm{dB}] \quad (1)$$

Signal attenuation under free-space conditions is calculated in Eq. 2 according to the carrier frequency f_c (GHz) and the distance d_{sat} (m), where R_E denotes Earth radius. The term d_{sat}, shown in Eq. 3, is computed as the 3GPP reports in [2].

$$L_{FS} = 20\,\log_{10}(d_{sat}) + 20\,\log_{10}(f_c) + 32.45\ \text{[dB]} \quad (2)$$

$$d_{sat} = \sqrt{R_E^2 \sin(\alpha_{sat})^2 + h_{sat}^2 + 2h_{sat}R_E} - R_E\,\sin(\alpha_{sat})\ \text{[m]} \quad (3)$$

The clutter loss L_C addresses the shadowing loss caused by surrounding buildings and objects. As shown in Eq. 4, the term is computed by the root mean square and comprises two components: a variable contribution accounting for the rooftop-to-street diffraction L_D and a constant attenuation derived from the reflection on the building on the opposite side of the street L_R. Both components are estimated independently and described below.

$$L_C = -10\,\log_{10}\left(10^{-\frac{L_D}{10}} + 10^{-\frac{L_R}{10}}\right)\ \text{[dB]} \quad (4)$$

The component loss L_R is calculated in Eq. 5 and accounts for the reflection loss in *Building 2* and the grazing diffraction in *Building 1*. The first part is computed based on a given reflection coefficient (Γ_R) and assuming the parity of the angles of incidence and reflection on *Building 2*. The diffraction-based loss ($L_{D,180°}$), with the obstruction just in line, is half of the value in free-space conditions, i.e. a loss of 6 dB.

$$L_R = -20\,\log_{10}(\Gamma_R) + L_{D,180°}\ \text{[dB]} \quad (5)$$

The diffraction-based contribution L_D is computed as a knife-edge diffraction loss by approximating *Building 1* as an ideal absorbing edge. For that purpose, we use the expression in Eq. 6 which accounts for an approximation of the Fresnel-Kirchoff loss $J(v)$ reported in [8, Eq. (30)].

$$L_D = 6.9 + 20\,\log_{10}\left(\sqrt{(v-0.1)^2+1} + v - 0.1\right)\ \text{[dB]} \quad (6)$$

The value of L_D, in Eq. 6, is considered valid for values of v greater than zero. The term v, defined in Eq. 7, is key to capture the dynamics of the model by adjusting the diffraction loss with regards to the position of the satellite, the knife-edge and the UE. Moreover, note that we tune v to depend on the wavelength λ, the slant range d_{sat} and the angular difference Δ_{sp}, which is defined as the absolute difference between the angles α_{sp} and α_{sat} in radians.

$$v = \sqrt{\frac{2}{\lambda}\,d_{sat}\,\alpha_1\,|\alpha_{sp} - \alpha_{sat}|} = \sqrt{\frac{2}{\lambda}\,d_{sat}\,\alpha_1\,\Delta_{sp}}\ [-] \quad (7)$$

For the estimation of the angle α_1, in Eq. 8, we use the approximation $r_1 \approx d_{sat}$, which is valid for values of $r_1 \gg r_2$.

$$\alpha_1 = \arctan(h/d_{sat})\ \text{[rad]} \quad (8)$$

We compute the height of the knife-edge (h) as follows:

$$h = h_{off}\,\sin(\Delta_{sp})\,\sqrt{1+\cot^2(\alpha_{sp})}\ \text{[m]} \quad (9)$$

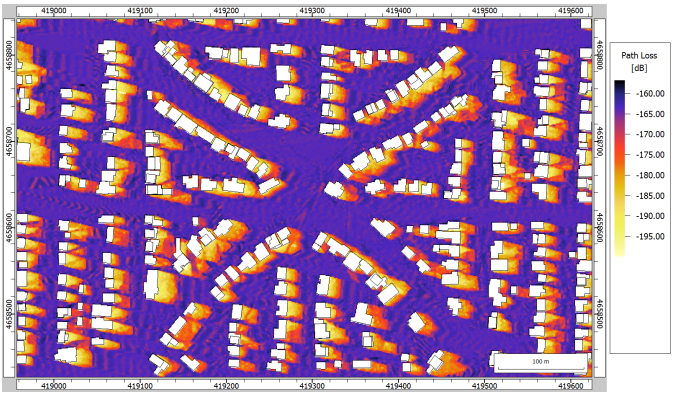

Fig. 2: Path loss map of Arlington Heights for a LEO satellite rising from North-West at 10° elevation angle and at 600 km height.

$$h_{off} = h_B - h_{UE}\ \text{[m]} \quad (10)$$

Further, the model considers log-normal shadow fading (χ) with zero mean and variance σ_χ^2, i.e. $\chi \sim N(0, \sigma_\chi^2)$, and as a function of the angular term Δ_{sp}. Further details are discussed in Section VI.

C. Model Discussion

In this section we have defined a model for the estimation of the large-scale aspects of the propagation. The small-scale fading caused by interference of multipath is out of the scope of this work and it is covered by 3GPP in [2].

Together with the work in [7], we address the novelty of modelling the time correlations of LEO-to-Ground satellite systems. The modelling is done as a function of the elevation angle instead of time to facilitate the calculations - we propose a geometrical model - and is based on the fact that time and space are intrinsically related.

The model automatically adjusts the propagation conditions and path loss according to values of α_{sat} and α_{sp}. The dynamics of the model have been checked to model elevation angles from 10° to 170°, as defined by the 3GPP in [2]. The angle α_{sp} may take any value in the application range of α_{sat}. We neglect the estimation of the horizontal distance from *Building 1* to the UE since it is self-contained in α_{sp}.

IV. Ray-Tracing Simulations

Ray-tracing simulations are conducted to validate the theoretical model as well as to study LEO-to-Ground signal propagation. Similarly as in [7], we simulate a suburban environment since we consider suburban and rural key scenarios for NTNs. For that purpose, we use a map of Arlington Heights village (western Chicago) with scattered low residential houses, an area of 840 m × 780 m and a maximum building height of 10 m. Despite ray-tracing is a valid tool for validation, real measurements can be useful to refine the model and enable further scenarios. Therefore, further study is encouraged to gain more insight on the topic.

The simulations are done in WinProp [12] using 3D intelligent ray-tracing, considering a limit of 2 diffractions and 1 reflection per ray with a spatial pixel resolution of 1 m. We

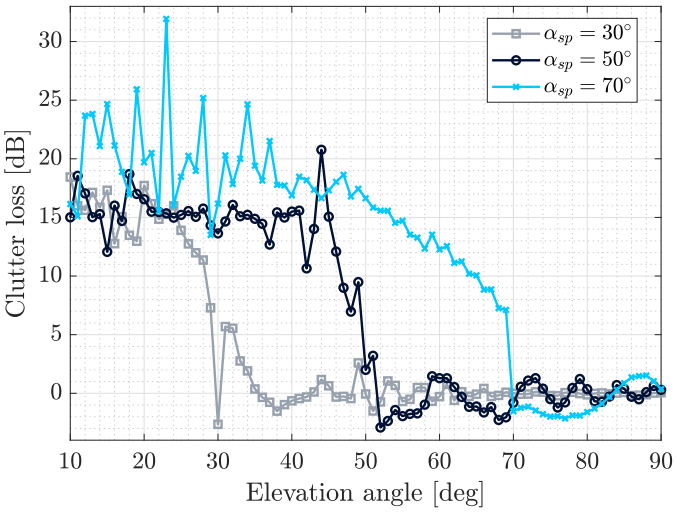

Fig. 3: Ray-tracing simulated clutter loss traces as a function of the elevation angle, at three different locations with non line-of-sight to line-of-sight transitions at 30°, 50° and 70° elevation angle.

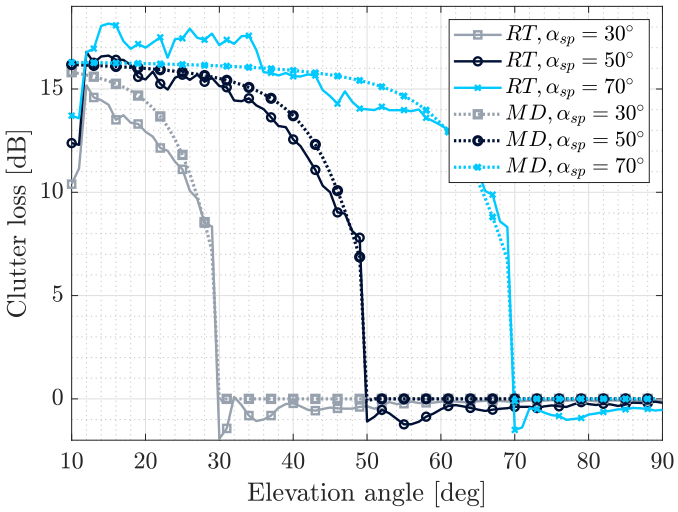

Fig. 4: Average clutter loss traces from ray-tracing (RT) and model (MD) for non line-of-sight to line-of-sight transitions at 30°, 50° and 70° elevation angle.

use a limitation of 10 rays per pixel and set a carrier frequency of 2 GHz. We compute time traces of the received power at outdoor pixels at 1.5 m height. A LEO satellite flies over the area at an altitude of 600 km and at elevation angles ranging from 10° to 170°.

We simulate the received power (P_{RX}) over roughly 456 000 pixels, where the contribution of each ray is coherently superposed. The path loss at the i^{th} pixel is calculated by considering isotropic transmitter power $P_{TX} = 10$ W. Fig. 2 shows the path loss heat-map of one of the simulations considering a transmitting LEO satellite at an altitude of 600 km with coordinates 44° N and 109° W, which corresponds to an elevation angle of 10°. From the resulting path loss, the clutter loss at the i^{th} pixel location can be estimated as detailed below.

$$CL_i = P_{TX,i} - P_{RX,i} - L_{FS,i} \quad \text{[dB]} \quad (11)$$

Fig. 3 shows the angular clutter loss variations at a given location as the LEO satellite flies over the scenario varying its α_{sat}. The traces, obtained from the ray-tracing data, correspond to locations with different NLOS/LOS angular transition characteristics, i.e. switching points α_{sp} at 30°, 50° and 70°.

V. Validation of the Model

This section presents the validation of the time-correlated geometrical model against ray-tracing simulations for a carrier frequency of 2 GHz. To that end, we tune the model by considering a building height of $h_B = 6$ m and a UE placed at $h_{UE} = 1.5$ m. To choose the building height value we consider two-storey houses with an average floor height of 3 m, which is well in line with the average building profiles in suburban areas. The satellite is at an altitude of 600 km with α_{sat} ranging from 10° to 90°. We account a constant value of 16.45 dB for L_R (Eq. 5) by considering a reflection coefficient of $|\Gamma_R| = 0.3$ and $L_{D,180°} = 6$ dB.

The model is compared against the ray-tracing simulations described in Section IV in terms of mean clutter loss. For illustrative purposes, we compute the clutter loss L_C using Eq. 4 for three switching points; $\alpha_{sp} = 30°, 50°, 70°$. Regarding the ray-tracing, we average the clutter loss values from all locations in the scenario that have the same switching angle. Fig. 4 shows the predicted and the simulated mean clutter loss as a function of α_{sat}. As one can observe, the model predicts the same trend observed in the ray-tracing. The traces follow a similar pattern which can be split in two stages. A first part where the clutter loss at low elevation angles remains constant or falls gently, showing a loss response around 15–18 dB. The second part begins approximately 20° before the NLOS-LOS transition where the loss value decreases steadily until the switching point, i.e. $\alpha_{sat} = \alpha_{sp}$. For values of $\alpha_{sat} \geq \alpha_{sp}$, the model predicts exactly 0 dB, while the ray-tracing traces show values near 0 dB. By analysing the propagation of the rays in the simulations, we observe that these effects are physically consistent if we consider that the reflected ray is the dominant for low elevation angles. Then, as long as the satellite rises, the rooftop-to-street diffraction gains relevance until the switching point, where the UE is no longer obstructed.

Even though the 3GPP model do not support satellite's mobility, another aspect to underline is the close conformity between the clutter loss obtained with our model and the clutter loss for suburban and rural scenarios, in the range of 16–19 dB, reported in [2, Table 6.6.2-3].

To quantify the accuracy of the model we calculate the root mean square error (RMSE). Regarding traces where α_{sp} ranges from 20° to 80°, the RMSE is in the range of 0.9–1.5 dB with a mean of 1.1 dB. The maximum RMSE is observed at $\alpha_{sp} = 80°$ and is due to the low number of NLOS to LOS transitions at high elevation angles.

VI. Modelling of the Shadow Fading

This section analyses and models the shadow fading χ as a function of $\Delta_{sp} = |\alpha_{sp} - \alpha_{sat}|$ and is based on the ray-tracing simulations. We compute the shadow fading samples

Angular distance	std deviation σ_χ (dB)		Decorrelation distance α_{corr} (°)	
Δ_{sp} (°)	LOS	NLOS	LOS	NLOS
10	2.3	4.2	2.6	2.5
20	1.4	5.1	2.8	3.1
30	1.1	5.6	2.9	4.5
40	0.9	6.1	2.9	6.4
50	0.6	6.2	3.0	8.7
60	0.4	6.5	3.1	10.5
70	0.3	7.1	3.1	11.9
80	0.3	7.4	3.2	12.6

TABLE I: Shadow fading parameters for non line-of-sight conditions modeled from the ray-tracing simulations.

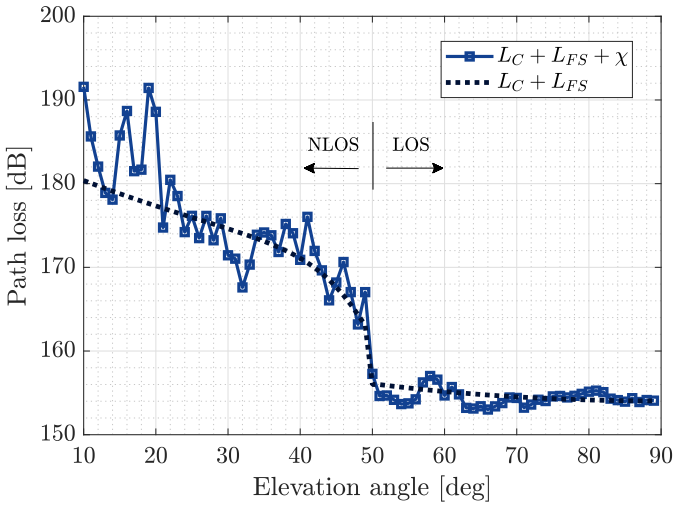

Fig. 5: Time-correlated overall path loss trace including free-space path loss, clutter loss and shadow fading for a user transitioning from non line-of-sight to line-of-sight at 50° elevation angle.

with the procedure detailed as follows. We first create a grid SF composed by the path loss values from each pixel location. SF is generated per elevation angle and the samples are labeled with regards to the LOS conditions. Discerning between NLOS and LOS pixels, we subtract the mean path loss to the individual samples of SF. As a result, we obtain distributions per elevation angle and LOS conditions. Such approach assumes that all pixels at a given elevation angle are at the same distance d_{sat} from the satellite, which dominates over any ground distance.

The analysis of the processed data shows that $\sigma_{\chi,nlos}$ decreases as Δ_{sp} decreases. Table I reflects the standard deviation of the shadow fading (σ_χ) as a function of Δ_{sp} with a 10° step, where σ_χ is taken from the nearest reference value of Δ_{sp}. It is worth noting that values of σ_χ for LOS conditions are in the range of 0.3–2.3 dB. Compared with NLOS conditions, this results in a lower impact when modelling as a function of Δ_{sp}.

Table I also provides the decorrelation distance (α_{corr}). Typically in system-level simulations, shadow fading is computed independently in time. However, the shadow fading effect of the same radio link is usually highly correlated. In a similar fashion, we model this parameter as a function of Δ_{sp}. For that purpose, we compute the autocorrelation function of the shadow fading ($R(\Delta_{sp}, \Delta_{sp}-\tau)$) and estimate α_{corr} for those values of α_{sat} that meets the condition $R = 1/e$ based on [13].

Fig. 5 depicts a time-correlated trace generated by the complete channel model. Firstly, the LOS model in [7] defines the channel states of a LEO-to-Ground link with a NLOS-LOS transition at 50°. Secondly, the model computes the mean path loss split in two parts: the free-space and the clutter components, as described in Section III. Finally, the correlated shadow fading is generated and applied accordingly.

VII. Conclusions

In this paper we have presented a model which captures the time-varying radio propagation conditions for low-Earth orbit satellite-to-ground links. We have analysed the large-scale changes of the received signal's power caused by obstructions appearing in the line-of-sight path due to the movement of the satellite. We have proposed a model that predicts the overall path loss discerning between free-space path loss, clutter loss and shadow fading. For the modelling of the clutter loss we have extended a combination of existing models for terrestrial deployments by including the full range of motion of a satellite in terms of elevation angle dependency. Furthermore, the model is geometry-based and it can be tuned accordingly. The results show a close agreement between the mean clutter loss from the designed model and the ray-tracing with an average root mean square error of 1.1 dB, regardless at what elevation angle the channel state transition occurs. The model can be conveniently used for system-level simulations targeting LEO satellite-to-Ground mobility aspects.

References

[1] G. Denis et al., "From New Space to Big Space: How Commercial Space Dream is Becoming a Reality," *Acta Astronautica*, 2020.

[2] 3GPP, "Study on New Radio (NR) to support Non-Terrestrial Networks (Release 15)," TR 38.811 V15.2.0, Sept. 2019.

[3] 3GPP, "Solutions for NR to support Non-Terrestrial Networks (NTN) (Release 16)," TR 38.821 V1.0.0, Dec. 2019.

[4] 3GPP, "Solutions for NR to support Non-Terrestrial Networks (NTN) (Release 17)," RP-202908, 3GPP TSG RAN Meeting 90-e, Dec. 2020.

[5] ITU, "Propagation data required for the design systems in the land mobile-satellite service," Rec. ITU-R P.681-11, 2019.

[6] E. Juan, M. Lauridsen, J. Wigard, and P. Mogensen, "5G New Radio Mobility Performance in LEO-based Non-Terrestrial Networks," *IEEE GLOBECOM*, 2020.

[7] E. Juan *et al.*, "A Time-correlated Channel State Model for 5G New Radio Mobility Studies in LEO Satellite Networks," *IEEE VTC-Spring*, 2021.

[8] ITU, "Propagation by diffraction," Rec. ITU-R P.526-15, 2019.

[9] F. Ikegami *et al.*, "Propagation Factors Controlling Mean Field Strength on Urban Streets," *IEEE Transactions on Antennas and Propagation*, 1984.

[10] J. Walfisch and H. Bertoni, "A Theoretical Model of UHF Propagation in Urban Environments," *IEEE Transactions on Antennas and Propagation*, 1988.

[11] E. Damosso and L. Correia, "Digital mobile radio towards future generation systems communications. cost 231 final report," *CEC*, 1999.

[12] Altair HyperWorks. WinProp propagation modelling. [Online]. Available: https://altairhyperworks.com/product/FEKO/WinProp-Propagation-Modeling

[13] M. Gudmundson, "Correlation model for shadow fading in mobile radio systems," *Electronics letters*, vol. 27, no. 23, pp. 2145–2146, 1991.